

Cite this: *Chem. Sci.*, 2018, 9, 6017

All publication charges for this article have been paid for by the Royal Society of Chemistry

Mechanisms of catalytic reduction of CO₂ with heme and nonheme metal complexes

Shunichi Fukuzumi, ^{ab} Yong-Min Lee, ^{ac} Hyun S. Ahn ^{ad} and Wonwoo Nam ^{ae}

The catalytic conversion of CO₂ into valuable chemicals and fuels has attracted increasing attention, providing a promising route for mitigating the greenhouse effect of CO₂ and also meeting the global energy demand. Among many homogeneous and heterogeneous catalysts for CO₂ reduction, this mini-review is focused on heme and nonheme metal complexes that act as effective catalysts for the electrocatalytic and photocatalytic reduction of CO₂. Because metalloporphyrinoids show strong absorption in the visible region, which is sensitive to the oxidation states of the metals and ligands, they are suited for the detection of reactive intermediates in the catalytic CO₂ reduction cycle by electronic absorption spectroscopy. The first part of this review deals with the catalytic mechanism for the one-electron reduction of CO₂ to oxalic acid with heme and nonheme metal complexes, with an emphasis on how the formation of highly energetic CO₂^{•−} is avoided. Then, the catalytic mechanism of two-electron reduction of CO₂ to produce CO and H₂O is compared with that to produce HCOOH. The effect of metals and ligands of the heme and nonheme complexes on the CO or HCOOH product selectivity is also discussed. The catalytic mechanisms of multi-electron reduction of CO₂ to methanol (six-electron reduced product) and methane (eight-electron reduced product) are also discussed for both electrocatalytic and photocatalytic systems.

Received 19th May 2018
Accepted 26th June 2018

DOI: 10.1039/c8sc02220h

rsc.li/chemical-science

^aDepartment of Chemistry and Nano Science, Ewha Womans University, Seoul 03760, Korea. E-mail: fukuzumi@chem.eng.osaka-u.ac.jp; yomlee@ewha.ac.kr; wwnam@ewha.ac.kr

^bGraduate School of Science and Engineering, Meijo University, Nagoya, Aichi 468-8502, Japan

^cResearch Institute for Basic Sciences, Ewha Womans University, Seoul 03760, Korea

^dDepartment of Chemistry, Yonsei University, Seoul 03722, Korea. E-mail: ahnhs@yonsei.ac.kr

^eSchool of Chemistry and Chemical Engineering, Shaanxi Normal University, Xi'an 710119, P. R. China



Shunichi Fukuzumi earned a bachelor's degree and a Ph.D. degree in applied chemistry from the Tokyo Institute of Technology in 1973 and 1978, respectively. After working as a postdoctoral fellow from 1978 to 1981 at Indiana University in USA, he became an Assistant Professor in 1981 at Osaka University where he was promoted to a Full Professor in 1994. His research has been

focused on electron transfer chemistry, particularly artificial photosynthesis. He is currently a Distinguished Professor at Ewha Womans University, a Designated Professor at Meijo University, and a Professor Emeritus at Osaka University.



Yong-Min Lee received his M.S. and Ph.D. degrees in Inorganic Chemistry from Pusan National University, Republic of Korea, under the supervision of Professor Sung-Nak Choi in 1999. After he worked at the Magnetic Resonance Centre (CERM) at the University of Florence, Italy, as a Postdoctoral fellow and Researcher under the direction of Professors Ivano Bertini and Claudio Luchinat

from 1999 to 2005, he joined the Centre for Biomimetic Systems at Ewha Womans University, as a Research Professor in 2006. He is currently a Special Appointment Professor at Ewha Womans University since 2009.

1 Introduction

Solar-driven reduction of CO₂ has merited increasing attention due to the hike in the world-wide consumption of fossil fuels and the consequential escalation in the atmospheric CO₂ level.^{1–9} There have so far been extensive studies on solar-driven reduction of CO₂ (ref. 7–21) as well as electrocatalytic reduction^{22–36} and catalytic hydrogenation of CO₂ in aprotic solvents and also in water.^{37–51} Carbon dioxide can be reduced by one electron and one proton to produce a half equivalent of oxalic acid (H₂C₂O₄) with a standard reduction potential of –0.50 V vs. SHE [eqn (1)].^{26,52} The two-electron reduction of CO₂ with two protons affords formic acid (HCOOH) [eqn (2)] or CO and H₂O [eqn (3)] with the standard reduction potentials of –0.25 and –0.11 V, respectively.⁵² Carbon dioxide can be further reduced by four, six, and eight electrons with four, six, and eight protons to produce formaldehyde [HCHO: eqn (4)], methanol [CH₃OH: eqn (5)] or ethylene [C₂H₄: eqn (6)], and methane [CH₄: eqn (7)] with the standard reduction potentials of –0.07, +0.02 or +0.06 V, and +0.17 vs. SHE, respectively.⁵² Therefore, the standard reduction potential is anodically shifted with an increased number of electrons and protons for CO₂ reduction, indicating that the involvement of a higher number of electrons and protons favours the CO₂ reduction thermodynamically. However, because the kinetic barrier generally increases with an additional number of electrons and protons involved in the reaction, appropriate catalysts are required to facilitate turnovers.



Among many catalysts for CO₂ reduction, metalloporphyrinoid complexes are suitable for mechanistic studies, because metalloporphyrinoids such as heme have intense absorption bands, which are sensitive to the oxidation states of metals and porphyrinoid ligands.^{53–58} Not only heme but also nonheme metal complexes have merited significant interest as bioinspired catalysts, which are studied in many redox reactions.^{26,58–73} This review is intended to focus on the mechanisms of both electrocatalytic and photocatalytic reduction of CO₂ with heme and nonheme metal complexes. The catalytic mechanisms are discussed not only for the one-electron/one-proton and two-electron/two-proton reductions of CO₂ [eqn (1) and (3)] but also for multi-electron/multi-proton pathways [eqn (4)–(7)]. The electrocatalytic and photocatalytic efficiencies are discussed based on the overpotentials and quantum yields, respectively.

2 Catalytic one-electron reduction of CO₂ to oxalic acid

The standard one electron reduction potential of CO₂ to CO₂^{•–} is as negative as –2.21 V vs. SCE (=–1.97 V vs. SHE) in *N,N'*-dimethylformamide (DMF)⁷⁴ and –1.90 V vs. SCE in water.⁷⁵ The dimerization of CO₂^{•–} affords oxalate dianions (C₂O₄^{2–}).⁷⁶ Therefore, catalysts are required to avoid the formation of highly energetic CO₂^{•–} and secure a low energy pathway en route to oxalic acid.

Ag^{II} and Pd^{II} complexes of both 2,3,7,8,12,13,17,18-octaethylporphyrin (OEP) and 5,10,15,20-tetraphenylporphyrin (TPP) were reported to act as catalysts for one-electron reduction of CO₂ to produce oxalic acid in CH₂Cl₂ containing 0.10 M tetrabutylammonium fluoride (TBAF) at an applied potential of –1.65 and –1.80 V vs. SCE, respectively.⁷⁷ In comparison with



Hyun S. Ahn earned his undergraduate degrees in chemistry and chemical engineering from the University of Washington in Seattle (2008). He then pursued his Ph.D. studies at the University of California at Berkeley, in the field of inorganic chemistry under the supervision of Prof. T. Don Tilley. Upon conferral of his Ph.D. in 2013, Hyun continued his research as a postdoctoral scholar at the University of

Texas at Austin with Prof. Allen J. Bard. He is currently an assistant professor of chemistry at Yonsei University. Hyun's research interest spans across the fields of catalysis, photoelectrochemistry, bio-electrochemistry, and energy conversion technologies.



Wonwoo Nam earned his B.S. (Honours) degree in Chemistry from California State University, Los Angeles, and his Ph.D. degree in Inorganic Chemistry from the University of California, Los Angeles (UCLA) under the supervision of Professor Joan S. Valentine in 1990. After working as a post-doctoral fellow at UCLA for one year, he became an Assistant Professor at Hong Ik University

in 1991. In 1994, he moved to Ewha Womans University, where he is currently a Distinguished Professor. His current research has been focused on the dioxygen activation, water oxidation, and important roles of metal ions in bioinorganic chemistry.



$\text{Ag}^{\text{II}}(\text{TPP})$ and $\text{Pd}^{\text{II}}(\text{TPP})$, neither $\text{Cu}^{\text{II}}(\text{TPP})$ nor $\text{Ni}^{\text{II}}(\text{TPP})$ showed catalytic activity for the electrochemical CO_2 reduction.⁷⁷

In contrast to $\text{Cu}^{\text{II}}(\text{TPP})$, a dinuclear nonheme copper(II) complex ($[\mathbf{4}]^{4+}$) can catalyse the one-electron reduction of CO_2 in acetonitrile (MeCN) in the presence of LiClO_4 to produce lithium oxalate at an applied potential of -0.03 V vs. NHE.⁷⁸ The electrochemical reduction of $[\mathbf{4}]^{4+}$ at a cathodic peak potential (E_{pc}) of $+0.06$ V vs. NHE ($=+0.06$ V vs. SHE) produced a dinuclear copper(I) complex ($[\mathbf{1}]^{2+}$) that is oxidized in air selectively by CO_2 (rather than O_2) to yield a tetranuclear copper(II) complex containing two bridging CO_2 -derived oxalate groups ($[\mathbf{2}]^{4+}$) as shown in Scheme 1.⁷⁸ The treatment of the copper(II) oxalate complex in MeCN with a soluble lithium salt results in the quantitative precipitation of lithium oxalate.⁷⁸ DFT calculations suggest the catalytic mechanism (Scheme 2) in which one CO_2 molecule is first reduced cooperatively by two Cu(I) metals to

give a fully delocalized mixed-valence $\text{Cu}^{\text{I}}/\text{Cu}^{\text{II}}(\text{CO}_2^{\cdot-})$ radical anion intermediate, followed by further partial reduction of the metal-ligated CO_2 molecule and (metal-mediated) nucleophilic-like attack on the carbon atom of an incoming second CO_2 molecule to afford the dinuclear $\text{Cu}(\text{II})$ -oxalate product ($[\mathbf{2}]^{4+}$).⁷⁹

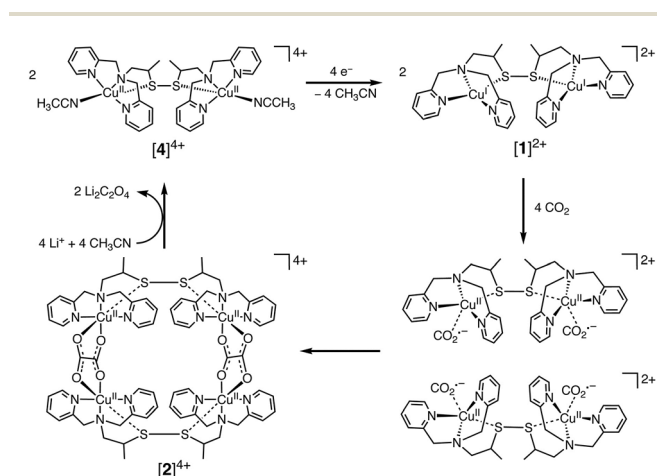
A binuclear metallacyclic copper complex was reported to be capable of selectively capturing CO_2 from air and reduce CO_2 to oxalate, in the form of an oxalate-bridged complex. The oxalate-bridged complex releases oxalic acid when it is treated with dilute mineral acid to regenerate the original copper complex.⁸⁰

It has also been reported that the one-electron reduction of chalcogen-bridged tricopper cyclophanates (Cu_3EL ; $\text{L}^{3-} = \text{tris}(\beta\text{-diketiminate})$; $\text{E} = \text{S}, \text{Se}$) (the one-electron reduction potential: $E_{\text{red}} = -0.89$ and -1.04 V vs. SCE, respectively) by CoCp_2^* (one-electron oxidation potential: $E_{\text{ox}} = -1.94$ V vs. Fc/Fc^+), $\text{FeCp}(\text{C}_6\text{Me}_6)$ ($E_{\text{ox}} = -2.07$ V vs. Fc/Fc^+), or KC_8 ($E_{\text{ox}} < -3.7$ V vs. Fc/Fc^+) in the presence of KPF_6 in DMF afforded $[\text{Cu}_3\text{EL}]^-$, which reacts with CO_2 to yield exclusively $\text{C}_2\text{O}_4^{2-}$ (95% yield, TON = 24) and regenerate Cu_3EL .⁸¹ Catalysis is observed employing KC_8 and $\text{FeCp}(\text{C}_6\text{Me}_6)$ as reductants, but only in the presence of KPF_6 .⁸¹

3 Electrocatalytic reduction of CO_2 to CO with metallocporphyrins

Iron tetraphenylporphyrin [$\text{Fe}(\text{TPP})$] (Fig. 1) was reported to catalyse the electrochemical reduction of CO_2 at the $\text{Fe}^{\text{I}}/\text{Fe}^{\text{0}}$ redox potential (-1.64 V vs. SCE) in DMF.⁸² However, the catalytic efficiency was very low and the catalytic activity of $\text{Fe}(\text{TPP})$ was rapidly lost during preparative-scale electrolysis.⁸² The addition of Mg^{2+} ions to the solution resulted in improved catalytic efficiency, resulting in a CO faradaic yield of ca. 60–70% and the rest in formate.⁸³ The presence of Lewis acids, such as Li^+ , Na^+ , Ba^{2+} , and Al^{3+} ions, also improved the catalytic efficiency. The addition of $\text{CF}_3\text{CH}_2\text{OH}$ (1.47 M) resulted in a large increase of the $\text{Fe}^{\text{I}}/\text{Fe}^{\text{0}}$ current to reach an $i_{\text{p}}/i_{\text{p}}^0$ value of 131.⁸² The $i_{\text{p}}/i_{\text{p}}^0$ value is given by eqn (8),

$$i_{\text{p}}/i_{\text{p}}^0 = 2.24(k_{\text{app}}[\text{CO}_2]RT/Fv)^{1/2} \quad (8)$$



Scheme 1 Catalytic one-electron reduction of CO_2 to oxalate with a dinuclear copper(I) complex ($[\mathbf{1}]^{2+}$). Reprinted with permission from ref. 78. Copyright 2010, The American Association for the Advancement of Science.



Scheme 2 Proposed catalytic cycle for one-electron reduction of CO_2 to oxalate with a copper(I) complex. Reprinted with permission from ref. 79. Copyright 2017, American Chemical Society.



Fig. 1 Iron tetraphenylporphyrin derivatives used for electrocatalytic reduction of CO_2 to CO. Reprinted with permission from ref. 86. Copyright 2012, The American Association for the Advancement of Science.



where k_{app} is the rate constant, R is the gas constant, T is the absolute temperature, F is the Faraday constant, and v is the scan rate.⁸³ The i_p/i_p^0 value was proportional to the concentration of CF_3CH_2OH at low concentrations, indicating that k_{app} exhibits second-order dependence on $[CF_3CH_2OH]$: $k_{app} \propto [CF_3CH_2OH]^2$.⁸³ Such second-order dependence of k_{app} on $[CF_3CH_2OH]$ suggests that the rate-determining step in the electrocatalytic reduction of CO_2 to CO involves a two-step protonation of the CO_2 adduct of $[PFe^{0}]^{2-}$ ($[PFe^{II}CO_2]^{2-}$) by AH to produce $[PFe^{II}CO]$ with dehydration as shown in Scheme 3, where $AH = CF_3CH_2OH$.^{83,84} The CO_2 adduct of an Fe^0 porphyrin ($[PFe^{II}CO_2]^{2-}$) was characterised by vibration at 590 cm^{-1} and CO bending mode at 806 cm^{-1} , which are both sensitive to ^{13}C substitution.⁸⁵ The $[PFe^{II}CO_2]^{2-}$ complex, which could only be observed at $-95\text{ }^\circ\text{C}$, was easily protonated by methanol even at $-80\text{ }^\circ\text{C}$ to produce $[PFe^{II}C(OH)O]^-$.⁸⁵

The electrocatalytic efficiency of CO_2 reduction to CO was improved by the introduction of phenolic groups in all *ortho* and *ortho'* positions of the phenyl groups of iron tetraphenylporphyrin.⁸⁶ The electrocatalytic reduction of CO_2 with iron 5,10,15,20-tetrakis(2',6'-dihydroxyphenyl)porphyrin (FeTDHPP in Fig. 1) in the presence of 2 M H_2O in CO_2 -saturated DMF ($[CO_2] = 0.23\text{ M}$) afforded a CO faradaic yield of 94% with a turnover number (TON) of 5.0×10^7 for 4 hours of electrolysis at -1.16 V vs. SHE with no observed degradation.⁸⁶ The average current density was 0.31 mA cm^{-2} that corresponds to a turnover frequency (TOF) of $3.2 \times 10^3\text{ s}^{-1}$ at an overpotential of 0.466 V , which is the most efficient among other CO_2 reduction catalysts.^{86–90} When the hydroxy groups in FeTDHPP were replaced by methoxy groups (FeTDMPP in Fig. 1), the catalytic activity of FeTDMPP was decreased by a factor of around 1 billion as compared to that of FeTDHPP with hydroxyl groups.⁸⁶ Therefore, the enhanced catalytic activity of FeTDHPP was attributed to the high local concentration of protons associated with the phenolic hydroxy substituents.⁸⁶

The introduction of four positively charged trimethylanilinium groups on the phenyl groups of iron tetraphenylporphyrin resulted in further improvement of the electrocatalytic activity

of CO_2 reduction by means of coulombic stabilization of the initial Fe^0-CO_2 adduct.⁸⁸ When four positively charged trimethylanilinium groups were introduced at the *ortho* positions of the TPP groups (Fe-*o*-TMA in Fig. 2), the maximum TOF was as high as 10^6 s^{-1} at a low overpotential of 0.220 V .⁸⁸ The catalyst standard potential (E_{cat}^0) of Fe-*o*-TMA was determined to be -0.944 V vs. SHE, which is the most positive ever reported for an iron porphyrin CO_2 -reduction catalyst.⁸⁸ The *para*-substituted analogue (Fe-*p*-TMA in Fig. 2) exhibited an E_{cat}^0 value of -1.263 V vs. SHE, which is much more negative than that of Fe-*o*-TMA, due to smaller coulombic stabilization of the initial Fe^0-CO_2 adduct.⁸⁸ The importance of the coulombic stabilization for the electrocatalytic activity of CO_2 reduction was further demonstrated by the introduction of four negatively charged sulfonate groups on the phenyl groups of iron tetraphenylporphyrin (Fe-*p*-PSULF in Fig. 2), which resulted in a more negative E_{cat}^0 value (-1.428 V vs. SHE).⁸⁸

In contrast to the electrocatalytic reduction of CO_2 in nonaqueous aprotic solvents such as DMF (*vide supra*), the electrocatalytic reduction of CO_2 in water always competes with the reduction of aqueous protons to hydrogen (H_2). The TOF of the electrocatalytic CO_2 reduction in an aqueous solution was reported to be much smaller compared to that in DMF solution because of the lower solubility of CO_2 in water.⁸⁸ A successful example of selective electrocatalytic reduction of CO_2 to CO over proton reduction was reported by employing Fe-*p*-TMA (Fig. 2) as a catalyst. This preparative-scale electrolysis was performed in water at pH 6.7 (adjusted by KOH addition) with an applied potential of -0.97 V vs. NHE for 4 h.⁸⁸ The average faradaic yields were CO (90%), H_2 (7%), acetate (1.4%), formate (0.7%) and oxalate (0.5%).⁸⁸ When pH was adjusted to 3.7 by the addition of 0.1 M formic acid buffer, the electrolysis with Fe-*p*-TMA resulted in the exclusive proton reduction to produce H_2 over the CO_2 reduction.⁸⁸

The selective electrocatalytic reduction of CO_2 to CO (over proton reduction) under acidic conditions was made possible with a cobalt(II) chlorin complex, $Co^{II}(Ch)$, adsorbed on multi-walled carbon nanotubes (MWCNTs) as a catalyst (Fig. 3).⁹¹



Scheme 3 Catalytic cycle for two-electron reduction of CO_2 to CO with an iron porphyrin ($[PFe]^{2-}$).⁸⁴

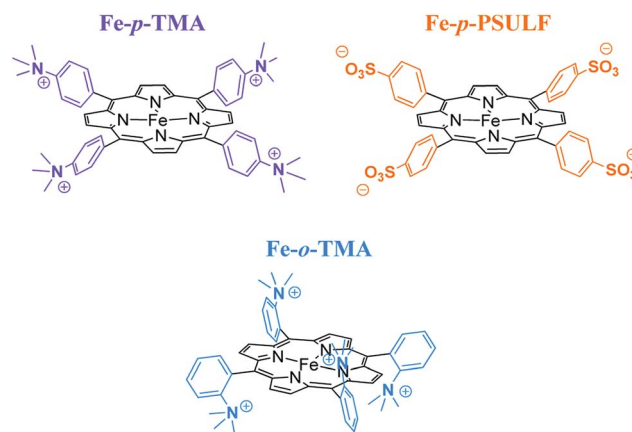


Fig. 2 Iron tetraphenylporphyrin derivatives with positive and negative charges used for electrocatalytic reduction of CO_2 to CO . Reprinted with permission from ref. 88. Copyright 2016, American Chemical Society.





Fig. 3 (a) Structure of $\text{Co}^{\text{II}}(\text{Ch})$ and (b) schematic image of $\text{Co}^{\text{II}}(\text{Ch})$ on MWCNTs. Reprinted with permission from ref. 91. Copyright 2015, Royal Society of Chemistry.

The electrolysis of a CO_2 -saturated aqueous solution (pH = 4.6 with Na_2SO_4) employing a glassy carbon working electrode modified with $\text{Co}^{\text{II}}(\text{Ch})$ @MWCNT (0.01 μmol) afforded mainly CO with a maximum TON of 1500 and TOF of 100 h^{-1} and little H_2 at -1.1 V vs. NHE ($= -1.34 \text{ V}$ vs. SCE).⁹¹ The faradaic yield of CO for the initial 2 h was determined to be as high as 89%, whereas that for H_2 production was only 11% at pH 4.6.⁹¹ The high selectivity for CO was maintained at pH 3.6, although H_2 became the main product at pH 2.0.⁹¹

When MWCNTs were replaced by reduced graphene oxide (rGO), which is a planar π -system, as a support material of $\text{Co}^{\text{II}}(\text{Ch})$, the CO yield became significantly smaller (TON = 350 for CO and 250 for H_2 at 20 h) (Fig. 4b) compared to that with



Fig. 4 Time profiles of the formation of CO and H_2 in the electrocatalytic reduction of CO_2 on a glassy carbon electrode modified with $\text{Co}^{\text{II}}(\text{Ch})$ (0.01 μmol) adsorbed on (a) MWCNTs (13 μg) and (b) rGO (13 μg) in a CO_2 -saturated aqueous solution (pH 4.6) containing Na_2SO_4 (5.0 mM) at an applied potential of -1.34 V vs. SCE. Reprinted with permission from ref. 91. Copyright 2015, Royal Society of Chemistry.

MWCNTs (Fig. 4a).⁹¹ Thus, the three dimensional assembly of MWCNTs with $\text{Co}^{\text{II}}(\text{Ch})$ (Fig. 3b) on the electrode surface is essential for the selective electrocatalytic reduction of CO_2 to CO.⁹¹ The π - π interaction between MWCNTs and $\text{Co}^{\text{II}}(\text{Ch})$ is presumed to provide a suitable hydrophobic environment for more selective binding of CO_2 over protons compared to the system with two-dimensional rGO as a support material.⁹¹

FeTDHPP (Fig. 1), a known CO_2 reduction catalyst in DMF, also exhibits electrocatalysis in a CO_2 -saturated aqueous solution (pH 7.3, NaHCO_3 0.5 M) at an applied potential of -1.03 V vs. NHE ($\eta = 480 \text{ mV}$), selectively producing CO over H_2 .⁹² A surface immobilisation tactic was implemented for the FeTDHPP catalyst on carbon surfaces by removing one phenyl group and appending a pyrene unit through a short linker.⁹² This immobilisation boosted both selectivity (96 : 4 CO : H_2 ratio) and overall conversion (97% total faradaic yield).⁹²

The cobalt phthalocyanine (CoPc) complex when adsorbed on MWCNTs was demonstrated to be an electrocatalyst for CO_2 reduction to CO at -0.63 V vs. RHE, with a remarkable TON of 9.7×10^4 and a faradaic yield exceeding 90%.⁹³ Compared to CoPc/MWCNT (2.5%), CoPc/rGO (2.2%) and CoPc/CB (3.3%) (CB: carbon black) exhibited less than one-third of the current density at -0.59 V vs. RHE with a 10% lower faradaic yield of CO and inferior stability.⁹³ The higher graphitic nature of CNTs compared to those of either rGO or CB allows stronger π - π interactions with CoPc and higher electron conduction, resulting in superior electrocatalysis.⁹³ A Pc/CNT hybrid without Co afforded a much lower faradaic yield for CO (only 19%), indicating that the Co centres in the CoPc/CNT act as the primary catalyst active sites.⁸⁵ Low but non-zero conversion of CO_2 to CO on Pc/CNT is attributed to the catalytic activity of Pc itself.⁹³

An iron tetraphenylporphyrin bearing six pendant OH groups in *ortho* and *ortho'* positions on three of the phenyl rings and one carboxylic acid group in the *para* position of the fourth phenyl was covalently attached to MWCNTs (CAT CO_2H , Scheme 4).⁹⁴ The covalent grafting of an Fe porphyrin on MWCNTs also led to efficient electrocatalytic reduction of CO_2 to CO selectively in water (pH 7.3) at an overpotential of 0.5 V.⁹⁴

Remarkably, the redox silent zinc(II) complex of 5,10,15,20-tetramesitylporphyrin (ZnTPP) was also reported as an effective electrocatalyst that afforded faradaic efficiencies as high as 95% for CO_2 reduction to CO at -1.7 V vs. SHE in DMF/ H_2O (9 : 1 v/v).⁹⁵ The UV-vis spectrum of the reduced ZnTPP species exhibits absorption bands at 710, 820, and 920 nm (Fig. 5, red line), which are the characteristic features of a transiently generated Zn complex with reduced ligands (*i.e.*, TPP').⁹⁵ ZnTPP' can react with CO_2 to regenerate ZnTPP and unidentified species.⁹⁵ The exact mechanism of the CO_2 reduction by ZnTPP' is yet to be clarified.

4 Electrocatalytic reduction of CO_2 to CO with nonheme metal complexes

A nonheme cobalt complex with a macrocyclic aminopyridine (I in Scheme 5) can also catalyse the electrochemical reduction of CO_2 to CO with a faradaic efficiency of $98 \pm 2\%$ and 1.22(1)





Scheme 4 An iron tetraphenylporphyrin bearing six pendant OH groups in *ortho* and *ortho'* positions on three of the phenyl rings and one carboxylic acid group in the *para* position of the fourth phenyl covalently attached to MWCNTs. Reprinted with permission from ref. 94. Copyright 2016, Royal Society of Chemistry.



Fig. 5 Absorption spectra of ZnTPP (black line), its reduced species (red line) produced by the reduction of ZnTPP by sodium naphthalenide, and the reduced species after exposure to CO₂ (blue line) or air (green line) in THF. Reprinted with permission from ref. 95. Copyright 2017, American Chemical Society.

million TON at an applied potential of -2.8 V in a DMF solution containing [ⁿBu₄N][PF₆] (0.1 M) and trifluoroethanol (1.2 M) under a CO₂ atmosphere.⁹⁶ When the pendant N–H group was replaced by a N–Me group, TONs became 300 times lower than that of **I**, indicating that the presence of the pendant NH moiety of the secondary amine is crucial for catalysis.^{96,97} Moreover, the presence of NH groups leads to a positive shift in the reduction potential of the Co^{II}/Co^I couple, resulting in a decrease in the overpotential for CO₂ reduction. Complex **I** is reduced by one electron to generate the Co^I complex, which is further reduced to the Co⁰ form. CO₂ binds to the Co⁰ complex to produce the



Scheme 5 Catalytic cycle of two-electron reduction of CO₂ to CO with a nonheme cobalt complex with a macrocyclic aminopyridine (**I**). Reprinted with permission from ref. 96. Copyright 2016, American Chemical Society.

CO₂ adduct ([Co(CO₂)]⁰, **III** in Scheme 5), which is stabilised by intramolecular H-bonds of the pendant secondary amines.⁹⁶ The successive protonation of the CO₂ complex affords CO and H₂O to regenerate complex **I**.^{96,97}

The [Co^{II}(qpy)(H₂O)₂]²⁺ (qpy = 2,2':6',2'':6'',2'''-quaterpyridine) complex also efficiently catalyses the electrochemical CO₂-to-CO conversion in an MeCN solution in the presence of weak Brønsted acids.⁹⁸ Controlled potential electrolysis (CPE) was performed at -1.1 V vs. SCE in the presence of 3 M PhOH, corresponding to 140 mV overpotential. CO was produced with 96% catalytic selectivity (a small amount of H₂ (4%) was obtained as the only byproduct) and 94% faradaic efficiency.⁹⁸ The [Co^{II}(qpy)(H₂O)₂]²⁺ complex is an excellent catalyst, at a very low overpotential, better than active Mn complexes (*vide infra*),^{99–103} being only surpassed by the Fe tetraphenylporphyrin bearing four trimethylammonium groups in the *ortho* position of each phenyl (complex **a** in Fig. 6).⁸⁸

Rhenium bipyridine complexes (Re(bpy)(CO)₃Cl and its derivatives)^{104–108} and manganese complexes (Mn(bpy)(CO)₃Br and its derivatives)^{109–114} are known to act as catalysts for electrocatalytic reduction of CO₂ to CO. The catalytic mechanisms have been investigated extensively using various spectroscopic methods including UV/Vis absorption and pulsed-EPR techniques (2P-ESEEM and HYSCORE) combined with DFT calculations.¹¹³ A key intermediate in the catalytic cycle of CO₂ reduction is demonstrated to be a low spin Mn^{II}-hydroxycarbonyl complex after the oxidative addition of CO₂ and H⁺ to a Mn⁰ carbonyl dimer (Scheme 6).¹¹³

The catalytic activity of a manganese complex *fac*-[MnBr(4,4'-bis(phosphonic acid)-2,2'-bipyridine)(CO)₃] (**MnP**) for CO production was improved when immobilized on a mesoporous TiO₂ electrode (TiO₂/**MnP**).¹¹⁴ Controlled potential electrolysis of TiO₂/**MnP** at $E_{\text{appl}} = -1.7$ V vs. Fc⁺/Fc ($\eta = 0.42$ V) under CO₂ in MeCN/H₂O (19/1) for 2 h passed an average charge of 1.10 ± 0.25 Coulombs with a faradaic efficiency of $67 \pm 5\%$ and a TON of 112 ± 17 for CO. The faradaic yield of H₂ for this system was $12.4 \pm 1.4\%$ and formate was not detected by ion chromatography.¹¹⁴



Fig. 6 Comparison of the metal catalysts (a,⁸⁸ b,⁹⁸ c,⁸⁸ d,⁹⁹ e,¹⁰⁰ f,¹⁰¹ g,¹⁰² and h¹⁰³) for the CO₂-to-CO electrochemical conversion in DMF or MeCN by means of their catalytic Tafel plots (log TOF as a function of the overpotential ($\eta = E^0(\text{CO}_2/\text{CO}) - E$). d' dotted lines: data for complex d in the presence of 0.1 M Mg²⁺.⁹⁹ ■: TOF value for b. Reprinted with permission from ref. 98. Copyright 2018, American Chemical Society.



Scheme 6 The catalytic cycle for two-electron reduction of CO₂ to CO with [Mn(bpy)(CO)₃]⁺. Reprinted with permission from ref. 113. Copyright 2014, WILEY-VCH Verlag GmbH.

The high activity and low overpotential of TiO₂/MnP are suggested to result from temporary desorption of the catalyst, followed by dimerization and re-anchoring within mesoporous TiO₂, because phosphonic acid modified molecules, such as MnP, display some lability when bound to TiO₂.¹¹⁵ The high local concentration of MnP may also place the metal centres in an environment where they are predisposed to dimerization upon reduction.¹¹⁴

The lowest overpotential for the electrocatalytic reduction of CO₂ to CO was achieved by using a manganese complex, [Mn{4,4'-di(1H-pyrrolyl-3-propyl carbonate)-2,2'-bipyridine}(CO)₃-MeCN]⁺(PF₆)⁻ loaded onto conductive MWCNTs ([Mn-MeCN]/MWCNT), which exhibited catalysis at -0.21 V vs. SHE (overpotential of about 100 mV for CO production).¹¹⁶ The MWCNTs

together with surface adsorbed K⁺ ions provided an environment to stabilize CO₂ adjacent to the Mn complex and significantly lowered the overpotential for CO₂ reduction in an aqueous solution.¹¹⁶

A case of selectivity tuning was observed as a function of ligand type when Ni(II) complexes in Fig. 7 were employed as catalysts for CO₂ reduction.¹¹⁷ Controlled potential electrolyses were carried out with each member of the catalyst series (Fig. 7) in CO₂-saturated MeCN solutions containing 2% H₂O.¹¹⁷ The 15-membered macrocyclic complex (3-Ni) gave high selectivity for CO₂ reduction to CO with a faradaic efficiency of 87%, the remaining 11% faradaic yield resulted in H₂ generation at an applied potential of 2.44 V vs. Fc^{+/0}.¹¹⁶ On the other hand, 1-Ni supported by a non-macrocyclic ligand gave a faradaic efficiency of 93% for H₂ and only 5% for CO, whereas the less rigid 16-membered macrocyclic complex (2-Ni) exhibited moderate selectivity for both CO (56%) and H₂ (43%) evolution in the presence of CO₂ and H₂O.¹¹⁷ Thus, increased rigidity of the redox-active macrocycle leads to enhanced selectivity for CO₂ reduction to CO over the competing hydrogen evolution reaction.¹¹⁷

The first electron reduction of 1-Ni is calculated to be that of the metal center and the second electron reduction is calculated to be ligand-based to produce the [Ni^I(L^{•-})] species. The [Ni^I(L^{•-})] complex reacts with H⁺ to form a metal hydride, from which H₂ is produced through a reaction with another H⁺.¹¹⁷ In contrast, the first and second reductions of 3-Ni are calculated to be both ligand-centered, and the resulting [Ni^{II}(L^{2•-})] complex is not capable of metal hydride generation, and therefore leads to no H₂ production. The two-electron reduced species of 2-Ni is best described by resonance forms [Ni^{II}(L^{2•-})] ↔ [Ni^I(L^{•-})], which are capable of producing both CO and H₂.¹¹⁷

A nickel complex supported by a pincer-type carbene-pyridine-carbene ligand also exhibited high selectivity for the electrocatalytic reduction of CO₂ to CO over proton reduction.¹¹⁸ A series of Ni^{II} macrocycle complexes structurally similar to [Ni(cyclam)]²⁺ (cyclam = 1,4,8,11-tetraazacyclotetradecane) also act as selective electrocatalysts for CO production over H₂ at a mercury pool working electrode in an aqueous solution.^{119–121} At pH 5, with an applied potential of -0.96 V vs. NHE (overpotential of -0.55 V), the Ni complexes are efficient, having high faradaic efficiencies for the selective reduction of CO₂ to CO.¹¹⁸ Hg provides favorable noncovalent dispersive interactions with the cyclam ligand to destabilise the poisoned CO-bound form of the catalyst, leading to enhanced catalytic reactivity.¹²² The binding of CO₂ to Ni(I) complexes has been



Fig. 7 Nickel(II) catalysts supported by non-macrocyclic and macrocyclic bipyridyl-NHC ligands. Reprinted with permission from ref. 117. Copyright 2018, Royal Society of Chemistry.

extensively studied by pulse radiolysis measurements to demonstrate that the formation of the Ni(I)-CO₂ adduct is in equilibrium between the Ni(I) complex and free CO₂.^{123,124}

5 Electrocatalytic reduction of CO₂ to HCOOH with heme and nonheme metal complexes

The two-electron/two-proton reduction of CO₂ also affords formate (HCOO⁻) as well as CO.¹²⁵ The reduced metal complex (M⁻) may react directly with CO₂ to produce the M-CO₂⁻ adduct that is further reduced with H⁺ to evolve CO and H₂O (Scheme 7) as in the case of the iron porphyrin in Scheme 3.¹²⁵ Alternatively M⁻ can react with H⁺ to generate the hydride complex (MH) capable of direct reaction with a proton to produce H₂, or alternatively couple with CO₂ to produce HCOO⁻ (Scheme 7).¹²⁵ Whether the catalytic two-electron/two-proton reduction of CO₂ affords CO or HCOO⁻ depends on the interplay of metals and ligands of the implemented catalyst.¹²⁶

A series of metalloprotoporphyrins (MPPs in Fig. 8) were employed as catalysts for the electrochemical reduction of CO₂ in an aqueous solution. Formic acid was not obtained when CrPP, MnPP, CoPP and FePP were used as catalysts. In the case of CoPP, CO was produced selectively at pH 3 with high faradaic efficiency.¹²⁶ Exercising the reaction with InPP, CrPP, SnPP and GaPP as catalysts, no gaseous products other than H₂ were observed. When SnPP, InPP and RhPP were employed as



Scheme 7 The reaction pathway of two-electron reduction of CO₂ with a metal complex (M) to produce HCOO⁻ or CO. Reprinted with permission from ref. 125. Copyright 2017, American Chemical Society.



Fig. 8 Chemical structure of metalloprotoporphyrins (MPP). Reprinted with permission from ref. 126. Copyright 2017, Elsevier.

catalysts, however, significant amounts of formic acid were produced depending on the pH as shown in Fig. 9, where the faradaic efficiency of HCOO⁻ with InPP at pH 9.6 was optimal, reaching a value close to 70%.¹²⁶ At very low pHs, hydrogen evolution dominated, resulting in little or no HCOOH production.¹²⁶ At very alkaline pHs, the H₂ production also seemed to be dominant, leading to poor selectivity towards HCOO⁻.¹²⁶ The catalytic mechanisms for HCOO⁻ production with InPP, SnPP and RhPP have not yet been clarified.

In contrast to iron porphyrins that catalyse the two-electron reduction of CO₂ to CO (Scheme 1), a nonheme iron(III) chloride complex bearing a 6,6'-di(3,5-di-*tert*-butyl-2-hydroxybenzene)-2,2'-bipyridine (^{*tbu*}dhbpy) ligand, Fe(^{*tbu*}dhbpy)Cl, catalyses the electrochemical two-electron reduction of CO₂ to formate in the presence of phenol (0.50 M) as a proton source in DMF with a faradaic efficiency of 68 ± 4% together with H₂ as a minor product (30 ± 10% faradaic efficiency) and minimal CO (1.1 ± 0.3% faradaic efficiency) at -2.5 V vs. Fc/Fc⁺.¹²⁷ The first one-electron reduction of Fe(^{*tbu*}dhbpy)Cl (Fe^{III/II}; E⁰ = -0.89 V vs. Fc/Fc⁺) exhibited a Nernstian PhOH-dependent electrochemical response, which suggests that the reduction is coupled with protonation of a bound phenolate moiety of the ligand framework by a PhOH proton donor as shown in Scheme 8.¹²⁷ At the second reduction potential (E⁰ = -2.09 V vs. Fc/Fc⁺), a second protonation event occurs at the metal centre to produce the iron(III)-hydride complex. At the third reduction potential (E⁰ = -2.65 V vs. Fc/Fc⁺), the catalytic activity was observed in the presence of PhOH as a sacrificial proton donor when the Fe(II)-hydride complex reacts with CO₂ to produce the formate complex from which formate is released to regenerate the Fe(II) complex (Scheme 8).¹²⁷ A kinetic isotope effect (KIE) of 4.8 ± 0.9 was observed when PhOD is used instead of PhOH, indicating that the insertion of CO₂ into the Fe(II)-hydride complex is the rate-determining step.¹²⁷ Fe(II)-hydride complexes were reported to hydrogenate CO₂ to produce formate.¹²⁸⁻¹³⁰ An iron cluster hydride [HFe₄N(CO)₁₂]⁻ is also reported as an effective catalyst for the electrochemical reduction of CO₂ to formate under mild conditions of pH 7 buffered aqueous solution and an applied potential of -1.2 V vs. SCE.^{131,132}

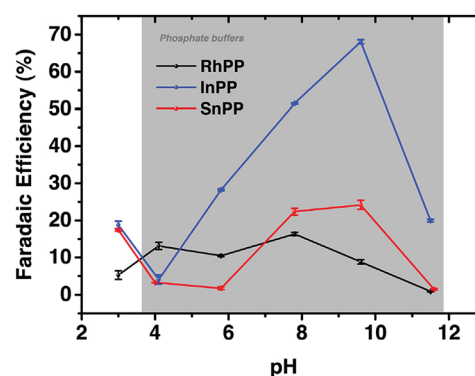


Fig. 9 Faradaic efficiencies for the electrocatalytic reduction of CO₂ to HCOOH or HCOO⁻ with RhPP, InPP and SnPP, determined at *t* = 10 min, at *E* = -1.5 V vs. RHE as function of pH. Reprinted with permission from ref. 126. Copyright 2017, Elsevier.



Scheme 8 Catalytic cycle for two-electron reduction of CO_2 to CO with a nonheme iron(III) chloride complex bearing a 6,6'-di(3,5-di-*tert*-butyl-2-hydroxybenzene)-2,2'-bipyridine ligand ($\text{Fe}^{\text{III}}(\text{t}^{\text{Bu}}\text{dhbpy})\text{Cl}$) via protonation by phenol. Reprinted with permission from ref. 127. Copyright 2018, American Chemical Society.

Cobalt complexes ($[\text{CpCo}(\text{P}_2\text{N}_2^{\text{R}})\text{I}]^+$) containing diphosphine ligands ($\text{P}_2\text{N}_2^{\text{R}}$) with two pendant amine residues catalyse the production of formic acid in DMF/water mixtures with a faradaic efficiency of $90 \pm 10\%$ at 500–700 mV overpotentials.¹³³ The $[\text{CpCo}(\text{P}_2\text{N}_2^{\text{R}})\text{I}]^+$ complex with $\text{R} = \text{cyclohexyl}$ and $\text{R}' = \text{benzyl}$ exhibited the best catalytic activity with a TON for HCOOH of 23 and 15 in the presence of 1.1 and 0.56 M water, respectively, after electrolyses at -2.25 V vs. Fc/Fc^+ for 1 h.¹³³ The electrocatalytic mechanism for CO_2 reduction to formate is proposed as shown in Scheme 9, where a Co^{II} -hydride intermediate hydrogenates CO_2 to produce formate. After two successive electron transfers, a Co^{I} species (complex III in Scheme 9) is generated. This species is then protonated and further reduced to form a cobalt(II)-hydride ($\text{Co}^{\text{II}}\text{-H}$) complex (complex V in Scheme 9).¹³³ DFT calculations indicated that the protonation of the pendant amine in either the Co^{II} or Co^{I} states allows two other pathways *via* intermediates III' and IV, respectively, through intramolecular proton transfer to the cobalt centre with the reduction of the metal center.¹³³ The $\text{Co}^{\text{II}}\text{-H}$ species V then reacts with CO_2 , generating complex VI. Internal hydride transfer from cobalt to CO_2 then yields complex VII.¹³³ The release of formic acid from complex VII regenerates the Co^{II} species (complex II in Scheme 9) and completes the catalytic cycle.¹³³

The product selectivity of electrocatalytic reduction of CO_2 to CO vs. HCOOH with the assembly of a $[\text{MnBr}(2,2'\text{-bipyridine})(\text{CO})_3]$ complex anchored to a carbon nanotube electrode *via* a pyrene unit was examined, and reported to be tuned by variation of metal complex density on the nanotube surface, where CO was observed as the main product at high catalyst loadings, and formate was the dominant CO_2 reduction product at low catalyst loadings.¹³⁴ The formation of a dimeric Mn^0 species at higher surface loading preferentially leads to CO formation, whereas at lower surface loading the electrochemical generation



Scheme 9 Catalytic cycle for two-electron reduction of CO_2 to CO with $[\text{CpCo}(\text{P}_2\text{N}_2^{\text{R}})\text{I}]^+$ complexes containing diphosphine ligands ($\text{P}_2\text{N}_2^{\text{R}}$) with two pendant amine residues. Reprinted with permission from ref. 133. Copyright 2017, American Chemical Society.

of a monomeric Mn -hydride is suggested to enhance the production of formate (Scheme 10).¹³⁴ The Mn -CNT hybrid catalyst exhibited much higher activity for electrocatalytic reduction of aqueous CO_2 with TONs of up to 1790 ± 290 for CO ($\eta = 550 \text{ mV}$) and up to 3920 ± 230 for formate ($\eta = 590 \text{ mV}$),¹³⁴ compared to electrolyses in the absence of carbon nanotubes.^{135–137}

When a Ni (bis-dithiolene) complex with a quinoxaline-pyran-fused dithiolene ligand (qpdt^{2-}) (see the X-ray crystal structure in Fig. 10) was employed as a CO_2 reduction catalyst using a Hg/Au amalgam electrode, formate as the major product together with minor amounts of CO and H_2 was observed at reasonable overpotentials with good faradaic yield and notable stability.¹³⁸ The onset potential of the catalytic wave with



Scheme 10 Two-electron reduction of CO_2 to CO vs. HCOOH with the $[\text{MnBr}(2,2'\text{-bipyridine})(\text{CO})_3]$ complex anchored to a carbon nanotube electrode *via* a pyrene unit depending on the surface concentration. Reprinted with permission from ref. 134. Copyright 2017, American Chemical Society.

$[\text{Ni}(\text{qpdt})_2]^-$ was observed at approximately -1.7 V vs. Ag/AgCl ($= -1.5$ V vs. SHE), with a halfwave potential at -1.80 V and a peak at -2 V.¹³⁸ The overpotential was determined to be ~ 340 mV by comparing the experimental onset potential to the standard potential of the CO_2/HCOOH couple in MeCN in the presence of trifluoroethanol as a proton source.¹³⁸ During the electrolysis, a complete reduction of the ligand occurred, followed by the subsequent pyran ring opening to produce the real catalyst ($[\text{Ni}^{\text{II}}(\text{L})_2]^{2-}$; L is a pyran ring-opened ligand produced from qpdt^{2-} by electrolysis) as shown in Scheme 11.¹³⁸ A Ni-hydride intermediate $[\text{Ni}^{\text{III}}(\text{H})(\text{L})_2]^{2-}$ was proposed to be a catalytically relevant species for CO_2 reduction to formate, which was produced by one-electron reduction of $[\text{Ni}^{\text{II}}(\text{L})_2]^{2-}$, followed by the reaction of $[\text{Ni}^{\text{I}}(\text{L})_2]^{3-}$ with H^+ .¹³⁸ The $[\text{Ni}^{\text{III}}(\text{H})(\text{L})_2]^{2-}$ species reacts with CO_2 , followed by a release of HCOO^- and regeneration of $[\text{Ni}^{\text{II}}(\text{L})_2]^{2-}$ upon the one-electron reduction at -0.51 V vs. Ag/AgCl.¹³⁸



Fig. 10 X-ray crystal structure of a Ni^{III} (bis-dithiolene) complex with a quinoxaline-pyran-fused dithiolene dianion ligand (qpdt^{2-}) ($[\text{Ni}^{\text{III}}(\text{qpdt})_2]^-$) at 50% probability. Hydrogen atoms are omitted for clarity. Reprinted with permission from ref. 138. Copyright 2018, American Chemical Society.



Scheme 11 Electrochemical reduction of $[\text{Ni}(\text{qpdt})_2]^-$, followed by the subsequent pyran ring opening to produce the real catalyst ($[\text{Ni}^{\text{II}}(\text{L})_2]^{2-}$; L is a pyran ring-opened ligand produced from qpdt^{2-} by electrolysis) during electrolysis. Reprinted with permission from ref. 138. Copyright 2018, American Chemical Society.

A small amount of CO observed during the electrolysis was proposed to be produced *via* the $\eta^1\text{-CO}_2$ species based on the DFT calculations.¹³⁸ Although many $\eta^2\text{-CO}_2$ nickel structures have been known to date,^{139–143} a rare $\eta^1\text{-}\kappa\text{C}$ binding mode of CO_2 to Ni was also reported by utilizing an anionic tridentate PNP ligand ($\text{PNP}^- = \text{N}[2\text{-P}^i\text{Pr}_2\text{-4-Me-C}_6\text{H}_3]_2^-$).^{144,145} The protonation of the $\eta^1\text{-CO}_2$ species affords the carboxylate intermediate ($[\text{Ni}(\text{C}(\text{O})\text{OH})(\text{L})_2]^{2-}$), which undergoes a heterolytic C–O bond cleavage to generate $[\text{Ni}(\text{CO})(\text{L})_2]^-$ upon protonation, followed by the release of CO.^{138,146}

6 Further electrocatalytic reduction of CO to fuels with metallocporphyrins

The electrochemical reduction of CO_2 to CO and its further reduction to methane were made possible by using a simple Co protoporphyrin molecular catalyst immobilized onto a pyrolytic graphite (PG) electrode (CoPP-PG).¹⁴⁷ In an aqueous solution with a pH value of 1, the faradaic efficiency for methane production is larger than that for CO, but the dominant product is H_2 .¹⁴⁷ At pH = 3, CO became a major product, especially at less cathodic potentials, where the faradaic efficiency for CO was 40%.¹⁴⁷ The efficiency towards CO can be further increased by performing the experiment at higher CO_2 pressure (10 atm), which leads to a faradaic efficiency of 60% at a potential of -0.6 V (Fig. 11).¹⁴⁷

The mechanism of catalytic CO_2 reduction to CO by CoPP may be similar to that of iron porphyrins in Scheme 1. The reduction of $\text{Co}^{\text{II}}\text{PP}$ to $[\text{Co}^{\text{I}}\text{PP}]^-$ is coupled with CO_2 binding to afford the CO_2 adduct that reacts with water to produce the $\text{Co}^{\text{III}}\text{PP-C}(\text{O})\text{OH}$ adduct, which is further reduced to produce the $\text{Co}^{\text{II}}\text{PP-CO}$ adduct as shown in Scheme 12.¹⁴⁷ The two-electron/two-proton reduction of the $\text{Co}^{\text{II}}\text{PP-CO}$ adduct affords the $\text{Co}^{\text{II}}\text{PP-HCHO}$ adduct that is further reduced by four electrons with four protons to finally yield methane and water, accompanied by the regeneration of $\text{Co}^{\text{II}}\text{PP}$ (Scheme 12).¹⁴⁷ The formation of CO is more favoured than H_2 at higher pHs.¹⁴⁷ However, further reduction of CO is more favoured at a low pH.¹⁴⁷ Thus, the faradaic yield of methane was higher than that of CO at pH 1, while H_2 remained the major product.¹⁴⁷

Crystallized copper phthalocyanine supported on carbon black (CuPc/CB) was reported to exhibit high selectivity for C_2H_4 with a maximum faradaic efficiency of 25% under atmospheric pressure at -1.6 V vs. Ag/AgCl ($= -1.4$ V vs. SHE), while CH_4 and CO were also generated as minor products (Fig. 12).¹⁴⁸ In contrast to the crystalline form of CuPc/CB, the noncrystalline CuPc/CB catalyst showed a much lower selectivity and reactivity for C_2H_4 production.¹⁴⁸ When noncrystalline CuPc was treated with Milli-Q water and chloroform to completely restore its crystallinity, the restored crystalline CuPc/CB catalyst afforded faradaic efficiency and partial current density values as high as those of the original crystalline CuPc/CB catalyst.¹⁴⁸ These results indicate that catalyst crystallinity is crucial for the selective conversion of CO_2 to C_2H_4 , because the C–C bond forming step to produce C_2H_4 from CO is likely mediated by two metal centers.¹⁴⁸





Fig. 11 Faradaic efficiency (FE) for the electrocatalytic CO_2 reduction to (a) CH_4 and (b) CO in 0.1 M perchlorate solution saturated with CO_2 conducted at each applied potential for 1 h and 90 min at P_{CO_2} = 1 atm and 10 atm, respectively [yellow bars: pH = 1, P_{CO_2} = 1 atm; blue bars: pH = 1, P_{CO_2} = 10 atm; magenta bars: pH = 3, P_{CO_2} = 1 atm and black bars pH = 3, P_{CO_2} = 10 atm]. Reprinted with permission from ref. 147. Copyright 2015, Nature Publishing Group.



Fig. 12 Products derived from CO_2 electrochemical reduction by crystalline CuPc/C at -1.6 V vs. Ag/AgCl in a two-compartment H-cell. Reprinted with permission from ref. 148. Copyright 2017, American Chemical Society.



Fig. 13 Schematic illustration of supramolecular assembly of cages between molecular components and supramolecular assembly of cages between molecular components and a copper electrode. Reprinted with permission from ref. 149. Copyright 2017, American Chemical Society.



Scheme 12 Catalytic cycle for two electron reduction of CO_2 to CO and further reduction to CH_4 with a Co protoporphyrin molecular catalyst (CoPP) immobilized onto a pyrolytic graphite (PG) electrode (CoPP-PG). Reprinted with permission from ref. 147. Copyright 2015, Nature Publishing Group.

Heterobimetallic cavities formed by the face-to-face coordination of thiol-terminated iron porphyrins on copper electrodes *via* self-assembly of supramolecular cages ($M = \text{Fe}$ in Fig. 13)

have made it possible to convert CO to C_2 products *via* C-C bond formation in aqueous electrochemical CO reduction with high faradaic efficiency (83% total with 57% to ethanol) and current density (1.34 mA cm^{-2}) at a potential of -0.40 V vs. RHE.¹⁴⁹ The cage-functionalized electrodes afforded an order of magnitude improvement in both selectivity and activity for electrocatalytic CO reduction compared to their parent copper surfaces.¹⁴⁹ Control analogues that lack thiol binding groups as well as positional isomers favouring edge-on binding or direct van der Waals stacking exhibited reduced surface access and negligible CO over water reduction selectivity, suggesting the critical role of the three-dimensional pockets in catalysis, where the Fe centre can aid in the cooperative reduction of potential acetaldehyde intermediates.¹⁴⁹

7 Photocatalytic reduction of CO_2 with heme and nonheme metal complexes

The electrocatalytic reduction of CO_2 can be replaced by photocatalytic reduction using photocatalysts instead of electrocatalysts. For example, the selective electrocatalytic reduction of CO_2 to CO with a glassy carbon electrode modified with a cobalt(II) chlorin complex ($\text{Co}^{\text{II}}(\text{Ch})$) adsorbed on MWCNTs

(Co^{II}(Ch)/MWCNTs; see Fig. 3 for the schematic image) is replaced by the photocatalytic reduction of CO₂ with trimethylamine (TEA) using Co^{II}(Ch)/MWCNTs as a CO₂ reduction catalyst and [Ru^{II}(Me₂phen)₃]²⁺ (Me₂phen = 4,7-dimethyl-1,10-phenanthroline) as a sensitizer.¹⁵⁰ The photocatalytic mechanism of the CO₂ reduction is shown in Scheme 13, where electron transfer from TEA to the excited state of [Ru^{II}(Me₂phen)₃]²⁺ ([Ru^{II}(Me₂phen)₃]²⁺*; * denotes the excited state) occurs to produce TEA radical cations and [Ru^I(Me₂phen)₃]⁺ that reduces Co^{II}(Ch) to [Co^I(Ch)]⁻.¹⁵⁰ [Co^I(Ch)]⁻ reacts with CO₂ to produce the [(Ch)Co^{III}(CO₂)]⁻ complex that is protonated to produce Co^{II}(Ch)COOH, from which water is released by the protonation to produce the [Co^{III}(Ch)CO]⁺ complex.¹⁵⁰ After the CO release from the Co(III)CO complex, the Co(III) complex is reduced by TEA to regenerate Co^{II}(Ch). Hydrogen evolution simultaneously occurs as a side reaction, much like in the electrocatalytic case, because [Co^I(Ch)]⁻ can also react with H⁺ to produce the hydride complex [(Co^{III}(Ch)(H))], which then can couple to a H⁺ to produce H₂.¹⁵¹ The TON of the photocatalytic reduction was determined to be 710 with the ratio of CO to H₂ of 2.4 : 1 in 20 h when 5.0 μM of Co^{II}(Ch) and 1.0 mg of MWCNTs were used.¹⁵⁰ The π-π interaction between MWCNTs and Co^{II}(Ch) may provide a suitable hydrophobic environment for the selective binding of CO₂ over protons, because the binding of CO₂ to the Co(I) complex is required for the formation of CO (Scheme 13).¹⁵⁰

An iron tetraphenylporphyrin complex functionalized with trimethylanilinium groups (Fe-*p*-TMA in Fig. 2), which is an efficient and selective molecular electrocatalyst for converting CO₂ to CO,⁸⁸ can also act as an efficient catalyst in photocatalytic reduction of CO₂ to methane using Ir(ppy)₃ (ppy = phenylpyridine) as a dye under visible light irradiation at ambient temperature and pressure.^{152,153} The catalytic system, which was evaluated in an acetonitrile solution containing a photosensitizer (Ir(ppy)₃), sacrificial electron donor (TEA) and proton source (trifluoroethanol), operates stably under irradiation over several days to produce CO, CH₄, and H₂ with turnover numbers (and selectivities) of 367 (78%), 79 (17%) and 26 (5%), respectively in 107 h.¹⁵² These values correspond to a methane production rate of 763 μmol per hour per gram of catalyst (μmol h⁻¹ g⁻¹), which is larger than those obtained using other catalysts^{154–159} that generate methane from CO₂. Trifluoroethanol facilitates the C–O bond cleavage step as observed in the electrocatalytic

reduction of CO₂ (Scheme 3).⁸⁴ No other gaseous product, methanol, formaldehyde or formate was produced.¹⁵² Isotopic labelling experiments conducted under a ¹²CO₂ or a ¹³CO₂ atmosphere confirmed that methane was produced from CO₂. A two-step procedure, that first reduces CO₂ to CO and then reduces CO to further reduced species of CO, generates methane with a selectivity of up to 82% and a quantum yield (light-to-product efficiency) of 0.18%.¹⁵²

The photocatalytic mechanism for CO₂ reduction to methane is proposed as shown in Scheme 14, where the starting Fe^{III} porphyrin is reduced with three electrons by Ir(ppy)₃* to the catalytically active Fe⁰ species.¹⁵² The Fe⁰ species reduces CO₂ to CO through a two-step protonation of the Fe⁰ species by CF₃-CH₂OH with dehydration (right-hand iron cycle) as in the case of the electrocatalytic reduction of CO₂ to CO in Scheme 3, where AH = trifluoroethanol.⁸⁴ The CO produced binds to Fe^{II} and is further reduced by a total of six electrons by electron transfer from Ir(ppy)₃* and six protons to generate CH₄ (and H₂O), through a postulated Fe^I-formyl (Fe^ICHO) intermediate (left-hand iron cycle).¹⁵²

Not all photocatalytic systems employ separately a catalyst and a photosensitizer. Fe-*p*-TMA can also catalyse the photocatalytic reduction of CO₂ to CO with 1,3-dimethyl-2-phenyl-2,3-dihydro-1*H*-benzo[*d*]imidazole (BIH) selectively under visible light irradiation without the assistance of an additional photosensitizer.¹⁶⁰ BIH was reported to enhance the photocatalytic formation of CO from CO₂,^{161,162} due to its high reductive ability (*E*_{ox} = +0.33 V vs. SCE = +0.57 vs. SHE),¹⁶³ its fast deprotonation to BI⁻ once oxidized and its overall two-electron donation capacity (BI⁻ could be in turn easily oxidized to BI⁺).

BIH was also used as a sacrificial reductant together with triethanolamine (TEOA) for visible-light driven CO₂ reduction in MeCN using [Ru(bpy)₃]²⁺ (bpy = 2,2'-bipyridine) as a photosensitizer and a Cu^{II} complex bearing 2,2':6',2'':6'':2'''-quaterpyridine (qpy) ([Cu(qpy)]²⁺) as a selective reduction catalyst.¹⁶⁴ The photocatalytic reaction is greatly enhanced by the presence of H₂O (1–4% v/v), and a TON of >12 400 for CO



Scheme 13 Photocatalytic cycle for two-electron reduction of CO₂ to CO with a cobalt(II) chlorin complex (Co^{II}(Ch)) adsorbed on multi-walled carbon nanotubes (Co^{II}(Ch)/MWCNTs). Reprinted with permission from ref. 150. Copyright 2016, Royal Society of Chemistry.



Scheme 14 Photocatalytic cycles for two-electron reduction of CO₂ to CO and further reduction to CH₄ with Fe-*p*-TMA and Ir(ppy)₃. Reprinted with permission from ref. 152. Copyright 2017, Macmillan Publishers Limited, part of Springer Nature.

production has been achieved with 97% selectivity, which is among the highest of molecular 3d-metal CO₂ reduction catalysts.¹⁶⁴ It was confirmed that the photocatalyst remains homogeneous based on results from Hg poisoning and dynamic light scattering experiments.¹⁶⁴

BIH alone acts as an electron donor in the photocatalytic reduction of CO₂ to CO with a Ni(II) complex bearing an S₂N₂-type tetradentate ligand, [Ni^{II}(bpet)]²⁺ (bpet = bis(2-pyridylmethyl)-1,2-ethanedithiol), as a CO₂ reduction catalyst and [Ru(bpy)₃]²⁺ as a photosensitizer in a DMA/H₂O solution mixture (9 : 1 v/v) under a CO₂ atmosphere at 298 K.¹⁶⁵ In this photocatalytic system, the [Ni^{II}(bpet)]²⁺ complex showed a high TON exceeding 700 with a very high CO selectivity of >99% and a quantum yield of 1.42%.¹⁶⁵

Composite electrodes formed by a combination of an organic-semiconductor with a metal-porphyrinoid catalyst were also evaluated as photocatalysts for CO₂ reduction. Graphite carbon nitride (g-C₃N₄), which has frequently been used as an organic semiconductor photocatalyst,^{166–169} was modified with a carboxyl group of tetra(4-carboxyphenyl)porphyrin iron(III) chloride (FeTCPP) to prepare a g-C₃N₄ nanosheets/FeTCPP (g-C₃N₄/FeTCPP) heterogeneous catalyst. The material was then implemented for the photoreduction of CO₂ to CO with TEOA under visible light illumination in MeCN : H₂O : TEOA (3 : 1 : 1) (Scheme 15).¹⁷⁰ Similar to the case shown in Scheme 13, Fe^{III}TCPP was reduced by the photo-induced electrons produced in g-C₃N₄ nanosheets up to Fe⁰TCPP that reduced CO₂ to CO coupled with proton transfer, whereas the holes left in g-C₃N₄ nanosheets were reduced by TEOA.¹⁷⁰ A maximum rate of 6.52 mmol g^{−1} in 6 h and a selectivity up to 98% for CO production have been achieved using the g-C₃N₄/FeTCPP heterogeneous catalyst.¹⁷⁰

To further improve the catalytic performance of composite electrodes, rutile TiO₂ nanoparticles were employed as modifiers to enhance interfacial charge transfer between semiconducting carbon nitride nanosheets (NS-C₃N₄) and a catalyst (supramolecular Ru(II)–Re(I) binuclear complex (RuRe)).¹⁷¹ The RuRe/TiO₂/NS-C₃N₄ hybrid photocatalyzed CO₂ reduction to CO with high selectivity under visible light (λ > 400 nm) irradiation, exhibiting higher catalytic activity compared to an analogue without TiO₂ by a factor of 4, in terms of both the CO formation rate and the TON.¹⁷¹ The enhanced photocatalytic activity was attributed mainly to the prolonged lifetime of free and/or shallowly trapped electrons generated in TiO₂/NSC₃N₄ under

visible-light irradiation, as revealed by transient absorption spectroscopy.¹⁷¹

A case of metal porphyrinoid catalysis was reported in conjunction with an inorganic semiconductor photoanode, completing a full photoelectrochemical cell. The photoelectrochemical reduction of CO₂ was performed in a two-compartment cell composed of an FeO(OH)/BiVO₄/FTO photoanode and a Co^{II}(Ch)/MWCNT cathode, which are connected with conducting wire as an external circuit and separated by a Nafion membrane (Fig. 14).¹⁷² A photo-driven oxidation reaction (of water) occurs at the photoanode, and the generated electrons are transported through the external circuit, being supplied as reducing equivalents to the Co^{II}(Ch)/MWCNT catalyst at the cathode. The photocatalytic controlled potential electrolysis of a CO₂-saturated aqueous solution (pH 4.6) using a photoelectrochemical cell in Fig. 14 at an applied bias voltage of −1.3 V at the cathode *versus* the photoanode resulted in the formation of CO and H₂ as shown in Fig. 15a, where the CO yield is significantly higher than the H₂ yield.¹⁷² The maximum current efficiency for CO production for the initial 2 h was 83% at pH 4.6.¹⁷² The amount of O₂ produced in the photoelectrochemical oxidation of water is one-half of the amounts of the sum of CO and H₂ produced in the electrochemical reduction of CO₂ and H₂O on the cathode (Fig. 15b).¹⁷²

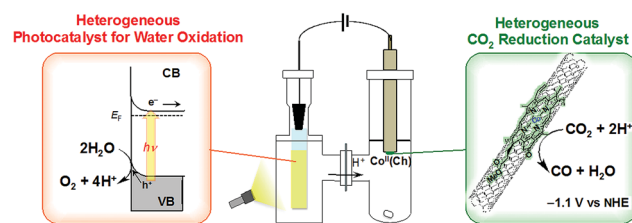


Fig. 14 Schematic illustration of a photoelectrochemical cell composed of an FeO(OH)/BiVO₄/FTO photoanode for the photocatalytic oxidation of water to O₂ and a Co^{II}(Ch)/MWCNT cathode for the catalytic reduction of CO₂ to CO. Cathode and anode compartments are separated by a Nafion membrane. Reprinted with permission from ref. 172. Copyright 2017, American Chemical Society.



Fig. 15 Time profiles of (a) the formation of CO (red circles) and H₂ (black circles) and (b) the formation of O₂ (blue circles) and CO plus H₂ (red circles) in the photo-assisted CPE with the Co^{II}(Ch)-modified cathode at an applied bias voltage of −1.3 V at the cathode *versus* the FeO(OH)/BiVO₄/FTO photoanode in a CO₂-saturated aqueous solution containing Na₂SO₄ (5.0 mM) at pH 4.6 under simulated 1 sun (AM 1.5G) illumination at 298 K. Reprinted with permission from ref. 172. Copyright 2017, American Chemical Society.



Scheme 15 Photocatalytic reduction of CO₂ to CO with TEOA using g-C₃N₄ nanosheets/FeTCPP (g-C₃N₄/FeTCPP). Reprinted with permission from ref. 170. Copyright 2018, Elsevier.





Scheme 16 Schematic illustration for the photocatalytic reduction of CO₂ to CO with the RuRe/CuGaO₂ electrode. Reprinted with permission from ref. 173. Copyright 2017, Royal Society of Chemistry.

A direct covalent linkage between a photosensitizer and a catalyst is a popular strategy due to the ease of electron transfer induced by proximity, and also one that is well suited for metal porphyrinoid catalysts owing to their synthetic versatility and flexibility. Such a case is shown in Scheme 16, where a Ru-based dye and a Re-based catalyst pair is synthesised and immobilised on a semiconductor surface. The photoelectrochemical reduction of CO₂ to CO was performed by using a RuRe/CuGaO₂ electrode under irradiation ($\lambda_{\text{ex}} > 460 \text{ nm}$), which can be selectively absorbed by the Ru photosensitizer unit of RuRe, in an aqueous solution containing NaHCO₃ (50 mM) saturated with CO₂ as shown in Scheme 16.¹⁷³ The difference in the observed current between the irradiation and dark conditions indicated that the cathodic photoresponse of the RuRe/CuGaO₂ electrode started at +0.30 V vs. Ag/AgCl (=+0.50 V vs. SHE), which was approximately 0.4 V more positive (due to the photovoltage supplied by the underlying semiconductor) than that of RuRe/NiO (*ca.* −0.1 V vs. Ag/AgCl = +0.1 V vs. SHE).¹⁷³ The TON for the formation of CO was 125 based on the RuRe loading, and the total faradaic efficiency for the production of CO plus H₂ was 81%.¹⁷³ The wavelength dependence of the incident-photon-to-current efficiencies of the RuRe/CuGaO₂ electrode agreed well with the absorption spectrum of the electrode, whereas the CuGaO₂ electrode alone (without the dye and catalyst) exhibited almost no photoresponse under irradiation ($\lambda_{\text{ex}} > 460 \text{ nm}$).¹⁷³ The photocurrent was generated by the injection of the electrons from the CuGaO₂ electrode into the excited Ru photosensitizer unit of RuRe, as shown in Scheme 16, because the flat band potential of the CuGaO₂ electrode in the reaction solution (+0.47 V vs. Ag/AgCl = +0.67 V vs. SHE) is less positive than the one-electron reduction potential of the excited state of RuRe ($E_{\text{red}} = +0.49 \text{ V vs. Ag/AgCl} = +0.69 \text{ V vs. SHE}$).¹⁷³

8 Conclusions

The one-electron reduction of CO₂ to oxalic acid is catalysed not only by metalloporphyrins such as Ag^{II}(TPP) and Pd^{II}(TPP) but

also by nonheme dicopper and tricopper complexes. Iron porphyrins act as efficient catalysts for both the electrocatalytic and photocatalytic reduction of CO₂ to CO in competition with the proton reduction to H₂. When four positively charged trimethylanilinium groups were introduced at the *ortho* positions of the TPP phenyls of an iron tetraphenylporphyrin (Fe-*o*-TMA in Fig. 2), the lowest overpotential of 0.220 V for CO₂ reduction to CO was achieved with a maximum TOF of 10⁶ s^{−1}. A variety of metal complexes such as cobalt and nickel complexes also act as effective catalysts for two-electron reduction of CO₂ to CO. When indium protoporphyrin was employed as an electrocatalyst, formate (HCOO[−]) was the main product instead of CO and the faradaic efficiency of HCOO[−] at pH 9.6 was close to 70%. Whether CO or HCOOH is produced depends on the metals and ligands of metalloporphyrins.

Further reduction of CO to methane has been made possible by using a Co protoporphyrin molecular catalyst immobilized onto a pyrolytic graphite (PG) electrode (CoPP-PG) in a purely aqueous electrolyte solution. The reduction of CO to C₂H₄ was also made possible by using crystallized copper phthalocyanine supported on carbon black (CuPc/CB) with a maximum faradaic efficiency of 25% under atmospheric pressure at −1.4 V vs. SHE, while CH₄ and CO were produced as minor products. The photocatalytic reduction of CO₂ to CO occurs in competition with the proton reduction to H₂ using triethylamine as a reductant, Co^{II}(Ch)/MWCNTs as a CO₂ reduction catalyst, and [Ru^{II}(Me₂phen)₃]²⁺ as a photosensitizer. When Fe-*p*-TMA with four positively charged trimethylanilinium groups introduced at the *para* positions of the TPP phenyls was employed as a catalyst, the photocatalytic reduction of CO using triethylamine as a reductant and Ir(ppy) afforded methane with a selectivity of up to 82% and a quantum yield of 0.18% under visible light irradiation at ambient temperature and pressure. Water can be used as an electron and proton source for the photocatalytic reduction of CO₂ to CO using a two-compartment cell composed of an FeO(OH)/BiVO₄/FTO photoanode and a Co^{II}(Ch)/MWCNT cathode. There are many reports on the photocatalytic reduction of CO₂ with water as an electron and proton source to produce CO, HCOOH and CH₄ using heterogeneous catalysts.^{174–184} It is highly desired to develop photocatalytic systems of CO₂ reduction to fuels such as ethylene, methanol and methane using water as an electron and proton source using homogeneous molecular catalysts as well.

Conflicts of interest

There are no conflicts to declare.

Acknowledgements

The authors gratefully acknowledge the contributions of their collaborators and coworkers cited in the listed references, and support through a SENTAN project (to S. F.) from the Japan Science and Technology Agency (JST), JSPS KAKENHI (No. 16H02268 to S. F.), the NRF of Korea through CRI (NRF-2012R1A3A2048842 to W. N.), GRL (NRF-2010-00353 to W. N.), and the Basic Science Research Program



(2017R1D1A1B03029982 to Y. M. L., 2017R1D1A1B03032615 to S. F., and 2017R1C1B2011074 to H. S. A.).

Notes and references

- N. S. Lewis, *Energy Environ. Sci.*, 2016, **9**, 2172–2176.
- M. Robert, *ACS Energy Lett.*, 2016, **1**, 281–282.
- Y. Zeng, J. Chen, T. Yu, G. Yang and Y. Li, *ACS Energy Lett.*, 2017, **2**, 357–363.
- J. Su and L. Vayssieres, *ACS Energy Lett.*, 2016, **1**, 121–135.
- J. M. Thomas and K. D. M. Harris, *Energy Environ. Sci.*, 2016, **9**, 687–708.
- N. S. Lewis, *Nat. Nanotechnol.*, 2016, **11**, 1010–1019.
- T. A. Faunce, W. Lubitz, A. W. Rutherford, D. MacFarlane, G. F. Moore, P. Yang, D. G. Nocera, T. A. Moore, D. H. Gregory, S. Fukuzumi, K. B. Yoon, F. A. Armstrong, M. R. Wasielewski and S. Styring, *Energy Environ. Sci.*, 2013, **6**, 695–698.
- S. Fukuzumi, *Joule*, 2017, **1**, 689–738.
- S. Perathoner and G. Centi, *Catal. Today*, 2018, DOI: 10.1016/j.cattod.2018.03.005.
- K. K. Sakimoto, N. Kornienko and P. Yang, *Acc. Chem. Res.*, 2017, **50**, 476–481.
- P. V. Kamat, *Acc. Chem. Res.*, 2017, **50**, 527–531.
- B. Wang, W. Chen, Y. Song, G. Li, W. Wei, J. Fanga and Y. Sun, *Catal. Today*, 2018, **311**, 23–39.
- K. Maeda, *Prog. Solid State Chem.*, 2018, DOI: 10.1016/j.progsolidstchem.2017.11.003.
- G. Zhao, X. Huang, X. Wang and X. Wang, *J. Mater. Chem.*, 2017, **5**, 21625–21649.
- Y. Zheng, W. Zhang, Y. Li, J. Chen, B. Yu, J. Wang, L. Zhang and J. Zhang, *Nano Energy*, 2017, **40**, 512–539.
- Y. Sohna, W. Huang and F. Taghipour, *Appl. Surf. Sci.*, 2017, **396**, 1696–1711.
- S. R. Lingampalli, M. M. Ayyub and C. N. R. Rao, *ACS Omega*, 2017, **2**, 2740–2748.
- X. Chang, T. Wang and J. Gong, *Energy Environ. Sci.*, 2016, **9**, 2177–2196.
- S. Wang and X. Wang, *Small*, 2015, **11**, 3097–3112.
- W. Kim, E. Edri and H. Frei, *Acc. Chem. Res.*, 2016, **49**, 1634–1645.
- Y. Tamaki and O. Ishitani, *ACS Catal.*, 2017, **7**, 3394–3409.
- J. Bonin, A. Maurin and M. Robert, *Coord. Chem. Rev.*, 2017, **334**, 184–198.
- H. Takeda, C. Cometto, O. Ishitani and M. Robert, *ACS Catal.*, 2017, **7**, 70–88.
- Y. Yang, S. Ajmal, X. Zheng and L. Zhang, *Sustainable Energy Fuels*, 2018, **2**, 510–537.
- C. Genovese, C. Ampelli, S. Perathoner and G. Centi, *Green Chem.*, 2017, **19**, 2406–2415.
- R. Francke, B. Schille and M. Roemelt, *Chem. Rev.*, 2018, **118**, 4631–4701.
- R. Daiyan, X. Lu, T. H. Ng and R. Amal, *ChemSusChem*, 2017, **10**, 4342–4358.
- B. Khezri, A. C. Fisher and M. Pumera, *J. Mater. Chem. A*, 2017, **5**, 8230–8246.
- Y. Zheng, J. Wang, B. Yu, W. Zhang, J. Chen, J. Qiao and J. Zhang, *Chem. Soc. Rev.*, 2017, **46**, 1427–1463.
- S. Ponnuram, I. V. Chernyshova and P. Somasundaran, *Adv. Colloid Interface Sci.*, 2017, **244**, 184–198.
- M. K. Brennaman, R. J. Dillon, L. Alibabaei, M. K. Gish, C. J. Dares, D. L. Ashford, R. L. House, G. J. Meyer, J. M. Papanikolas and T. J. Meyer, *J. Am. Chem. Soc.*, 2016, **138**, 13085–13102.
- A. J. Martín, G. O. Larrazábal and J. Pérez-Ramírez, *Green Chem.*, 2015, **17**, 5114–5130.
- C. Costentin, M. Robert and J.-M. Savéant, *Acc. Chem. Res.*, 2015, **48**, 2996–3006.
- K. Mase, S. Aoi, K. Ohkubo and S. Fukuzumi, *J. Porphyrins Phthalocyanines*, 2016, **20**, 935–949.
- J. Qiao, Y. Liu, F. Hong and J. Zhang, *Chem. Soc. Rev.*, 2014, **43**, 631–675.
- C. Costentin, M. Robert and J.-M. Savéant, *Chem. Soc. Rev.*, 2013, **42**, 2423–2436.
- K. Sordakis, C. Tang, L. K. Vogt, H. Junge, P. J. Dyson, M. Beller and G. Laurenczy, *Chem. Rev.*, 2018, **118**, 372–433.
- N. Onishi, G. Laurenczy, M. Beller and Y. Himeda, *Coord. Chem. Rev.*, 2018, DOI: 10.1016/j.ccr.2017.11.021.
- A. Álvarez, A. Bansode, A. Urakawa, A. V. Bavykina, T. A. Wezendonk, M. Makkee, J. Gascon and F. Kapteijn, *Chem. Rev.*, 2017, **117**, 9804–9838.
- W.-H. Wang, Y. Himeda, J. T. Muckerman, G. F. Manbeck and E. Fujita, *Chem. Rev.*, 2015, **115**, 12936–12973.
- S. Kattel, P. J. Ramírez, J. G. Chen, J. A. Rodriguez and P. Liu, *Science*, 2017, **355**, 1296–1299.
- S. Kattel, P. Liu and J. G. Chen, *J. Am. Chem. Soc.*, 2017, **139**, 9739–9754.
- P. Gao, S. Li, X. Bu, S. Dang, Z. Liu, H. Wang, L. Zhong, M. Qiu, C. Yang, J. Cai, W. Wei and Y. Sun, *Nat. Chem.*, 2017, **9**, 1019–1024.
- W. H. Bernskoetter and N. Hazari, *Acc. Chem. Res.*, 2017, **50**, 1049–1058.
- J. Klankermayer, S. Wesselbaum, K. Beydoun and W. Leitner, *Angew. Chem., Int. Ed.*, 2016, **55**, 7296–7343.
- D. Mellmann, P. Sponholz, H. Junge and M. Beller, *Chem. Soc. Rev.*, 2016, **45**, 3954–3988.
- A. M. Appel, J. E. Bercaw, A. B. Bocarsly, H. Dobbek, D. L. DuBois, M. Dupuis, J. G. Ferry, E. Fujita, R. Hille, P. J. A. Kenis, C. A. Kerfeld, R. H. Morris, C. H. F. Peden, A. R. Portis, S. W. Ragsdale, T. B. Rauchfuss, J. N. H. Reek, L. C. Seefeldt, R. K. Thauer and G. L. Waldrop, *Chem. Rev.*, 2013, **113**, 6621–6658.
- S. Fukuzumi and T. Suenobu, *Dalton Trans.*, 2013, **42**, 18–28.
- E. Fujita, J. T. Muckerman and Y. Himeda, *Biochim. Biophys. Acta*, 2013, **1827**, 1031–1038.
- Y. Maenaka, T. Suenobu and S. Fukuzumi, *Energy Environ. Sci.*, 2012, **5**, 7360–7367.
- S. Fukuzumi, *Eur. J. Inorg. Chem.*, 2008, 1351–1362.
- A. J. Bard, R. Parsons and J. Jordan, *Standard potentials in aqueous solutions*, CRC press, 1985.
- X. Huang and J. T. Groves, *Chem. Rev.*, 2018, **118**, 2491–2553.



- This journal is © The Royal Society of Chemistry 2018

- 107 T. W. Schneider, M. Z. Ertem, J. T. Muckerman and A. M. Angeles-Boza, *ACS Catal.*, 2016, **6**, 5473–5481.
- 108 M. L. Clark, P. L. Cheung, M. Lessio, E. A. Carter and C. P. Kubiak, *ACS Catal.*, 2018, **8**, 2021–2029.
- 109 Y. C. Lam, R. J. Nielsen, H. B. Gray and W. A. Goddard III, *ACS Catal.*, 2015, **5**, 2521–2528.
- 110 C. Riplinger and E. A. Carter, *ACS Catal.*, 2015, **5**, 900–908.
- 111 K. T. Ngo, M. McKinnon, B. Mahanti, R. Narayanan, D. C. Grills, M. Z. Ertem and J. Rochford, *J. Am. Chem. Soc.*, 2017, **139**, 2604–2618.
- 112 J. E. Vandezande and H. F. Schaefer III, *Organometallics*, 2018, **37**, 337–342.
- 113 M. Bourrez, M. Orio, F. Molton, H. Vezin, C. Duboc, A. Deronzier and S. Chardon-Noblat, *Angew. Chem., Int. Ed.*, 2014, **53**, 240–243.
- 114 T. E. Rosser, C. D. Windle and E. Reisner, *Angew. Chem., Int. Ed.*, 2016, **55**, 7388–7392.
- 115 F. Li, K. Fan, B. Xu, E. Gabrielsson, Q. Daniel, L. Li and L. Sun, *J. Am. Chem. Soc.*, 2015, **137**, 9153–9159.
- 116 S. Sato, K. Saita, K. Sekizawa, S. Maeda and T. Morikawa, *ACS Catal.*, 2018, **8**, 4452–4458.
- 117 X. Su, K. M. McCardle, J. A. Panetier and J. W. Jurss, *Chem. Commun.*, 2018, **54**, 3351–3354.
- 118 M. Sheng, N. Jiang, S. Gustafson, B. You, D. H. Ess and Y. Sun, *Dalton Trans.*, 2015, **44**, 16247–16250.
- 119 J. Schneider, H. Jia, K. Kobi, D. E. Cabelli, J. T. Muckerman and E. Fujita, *Energy Environ. Sci.*, 2012, **5**, 9502–9510.
- 120 M. Beley, J.-P. Collin, R. Ruppert and J.-P. Sauvage, *J. Am. Chem. Soc.*, 1986, **108**, 7461–7467.
- 121 M. Beley, J.-P. Collin, R. Ruppert and J.-P. Sauvage, *J. Chem. Soc., Chem. Commun.*, 1984, 1315–1316.
- 122 Y. Wu, B. Rudshiteyn, A. Zhanaidarova, J. D. Froehlich, W. Ding, C. P. Kubiak and V. S. Batista, *ACS Catal.*, 2017, **7**, 5282–5288.
- 123 J. Schneider, H. Jia, J. T. Muckerman and E. Fujita, *Chem. Soc. Rev.*, 2012, **41**, 2036–2051.
- 124 D. C. Grills, D. E. Polyansky and E. Fujita, *ChemSusChem*, 2017, **10**, 4359–4373.
- 125 N. D. Loewen, T. V. Neelakantan and L. A. Berben, *Acc. Chem. Res.*, 2017, **50**, 2362–2370.
- 126 Y. Y. Birdja, J. Shen and M. T. M. Koper, *Catal. Today*, 2017, **288**, 37–47.
- 127 A. W. Nichols, S. Chatterjee, M. Sabat and C. W. Machan, *Inorg. Chem.*, 2018, **57**, 2111–2121.
- 128 F. Bertini, N. Gorgas, B. Stöger, M. Peruzzini, L. F. Veiros, K. Kirchner and L. Gonsalvi, *ACS Catal.*, 2016, **6**, 2889–2893.
- 129 C. Federsel, A. Boddien, R. Jackstell, R. Jennerjahn, P. J. Dyson, R. Scopelliti, G. Laurenczy and M. Beller, *Angew. Chem., Int. Ed.*, 2010, **49**, 9777–9780.
- 130 C. Ziebart, C. Federsel, P. Anbarasan, R. Jackstell, R. Baumann, W. A. Spannenberg and M. Beller, *J. Am. Chem. Soc.*, 2012, **134**, 20701–20704.
- 131 A. Taheri, E. J. Thompson, J. C. Fettingner and L. A. Berben, *ACS Catal.*, 2015, **5**, 7140–7151.
- 132 A. Taheri, N. D. Loewen, D. B. Cluff and L. A. Berben, *Organometallics*, 2018, **37**, 1087–1091.
- 133 S. Roy, B. Sharma, J. Pécaut, P. Simon, M. Fontecave, P. D. Tran, E. Derat and V. Artero, *J. Am. Chem. Soc.*, 2017, **139**, 3685–3696.
- 134 B. Reuillard, K. H. Ly, T. E. Rosser, M. F. Kuehnel, I. Zebger and E. Reisner, *J. Am. Chem. Soc.*, 2017, **139**, 14425–14435.
- 135 A. Sinopoli, N. T. La Porte, J. F. Martinez, M. R. Wasielewski and M. Sohail, *Coord. Chem. Rev.*, 2018, **365**, 60–74.
- 136 J. J. Walsh, C. L. Smith, G. Neri, G. F. S. Whitehead, C. M. Robertson and A. J. Cowan, *Faraday Discuss.*, 2015, **183**, 147–160.
- 137 M. Stanbury, J.-D. Compain and S. Chardon-Noblat, *Coord. Chem. Rev.*, 2018, **36**, 120–137.
- 138 T. Fogeron, T. K. Todorova, J.-P. Porcher, M. Gomez-Mingot, L.-M. Chamoreau, C. Mellot-Draznieks, Y. Li and M. Fontecave, *ACS Catal.*, 2018, **8**, 2030–2038.
- 139 Y.-E. Kim, J. Kim and Y. Lee, *Chem. Commun.*, 2014, **50**, 11458–11461.
- 140 C. Yoo, Y.-E. Kim and Y. Lee, *Acc. Chem. Res.*, 2018, **51**, 1144–1152.
- 141 J. S. Anderson, V. M. Iluc and G. L. Hillhouse, *Inorg. Chem.*, 2010, **49**, 10203–10207.
- 142 R. Beck, M. Shoshani, J. Krasinkiewicz, J. A. Hatnean and S. A. Johnson, *Dalton Trans.*, 2013, **42**, 1461–1475.
- 143 M. Aresta, C. F. Nobile, V. G. Albano, E. Forni and M. Manassero, *J. Chem. Soc., Chem. Commun.*, 1975, 636–637.
- 144 C. Yoo and Y. Lee, *Chem. Sci.*, 2017, **8**, 600–605.
- 145 C. Yoo, J. Kim and Y. Lee, *Organometallics*, 2013, **32**, 7195–7203.
- 146 D. Sahoo, C. Yoo and Y. Lee, *J. Am. Chem. Soc.*, 2018, **140**, 2179–2185.
- 147 J. Shen, R. Kortlever, R. Kas, Y. Y. Birdja, O. Diaz-Morales, Y. Kwon, I. Ledezma-Yanez, K. J. P. Schouten, G. Mul and M. T. M. Koper, *Nat. Commun.*, 2015, **6**, 8177.
- 148 S. Kusama, T. Saito, H. Hashiba, A. Sakai and S. Yotsuhashi, *ACS Catal.*, 2017, **7**, 8382–8385.
- 149 M. Gong, Z. Cao, W. Liu, E. M. Nichols, P. T. Smith, J. S. Derrick, Y.-S. Liu, J. Liu, X. Wen and C. J. Chang, *ACS Cent. Sci.*, 2017, **3**, 1032–1040.
- 150 S. Aoi, K. Mase, K. Ohkubo and S. Fukuzumi, *Catal. Sci. Technol.*, 2016, **6**, 4077–4080.
- 151 S. Aoi, K. Mase, K. Ohkubo and S. Fukuzumi, *Chem. Commun.*, 2015, **51**, 15145–15148.
- 152 H. Rao, L. C. Schmidt, J. Bonin and M. Robert, *Nature*, 2017, **548**, 74–77.
- 153 C. Steinlechner and H. Junge, *Angew. Chem., Int. Ed.*, 2018, **57**, 44–45.
- 154 T. Wu, L. Zou, D. Han, F. Li, Q. Zhang and L. Niu, *Green Chem.*, 2014, **16**, 2142–2146.
- 155 B. Alotaibi, S. Fan, D. Wang, J. Ye and Z. Mi, *ACS Catal.*, 2015, **5**, 5342–5348.
- 156 X. Liu, S. Inagaki and J. Gong, *Angew. Chem., Int. Ed.*, 2016, **55**, 14924–14950.
- 157 Y. Wang, X. Bai, H. Qin, F. Wang, Y. Li, X. Li, S. Kang, Y. Zuo and L. Cui, *ACS Appl. Mater. Interfaces*, 2016, **8**, 17212–17219.
- 158 L. Yu, G. Li, X. Zhang, X. Ba, G. Shi, Y. Li, P. K. Wong, J. C. Yu and Y. Yu, *ACS Catal.*, 2016, **6**, 6444–6454.

- 159 H. Wang, Y. Chen, X. Hou, C. Ma and T. Tan, *Green Chem.*, 2016, **18**, 3250–3256.
- 160 H. Rao, J. Bonin and M. Robert, *Chem. Commun.*, 2017, **53**, 2830–2833.
- 161 Y. Tamaki, K. Koike, T. Morimoto and O. Ishitani, *J. Catal.*, 2013, **304**, 22–28.
- 162 Y. Kuramochi and O. Ishitani, *Inorg. Chem.*, 2016, **55**, 5702–5709.
- 163 E. Hasegawa, S. Takizawa, T. Seida, A. Yamaguchi, N. Yamaguchi, N. Chiba, T. Takahashi, H. Ikeda and K. Akiyama, *Tetrahedron*, 2006, **62**, 6581–6588.
- 164 Z. Guo, F. Yu, Y. Yang, C.-F. Leung, S.-M. Ng, C.-C. Ko, C. Cometto, T.-C. Lau and M. Robert, *ChemSusChem*, 2017, **10**, 4009–4013.
- 165 D. Hong, Y. Tsukakoshi, H. Kotani, T. Ishizuka and T. Kojima, *J. Am. Chem. Soc.*, 2017, **139**, 6538–6541.
- 166 W. J. Ong, L. L. Tan, Y. H. Ng, S. T. Yong and S. P. Chai, *Chem. Rev.*, 2016, **116**, 7159–7329.
- 167 L. Wang, R.-J. Xie, T. Suehiro, T. Takeda and N. Hirosaki, *Chem. Rev.*, 2018, **118**, 1951–2009.
- 168 M. Mousavi, A. Habibi-Yangjeh and S. R. Pouran, *J. Mater. Sci.: Mater. Electron.*, 2018, **29**, 1719–1747.
- 169 H. J. Yu, R. Shi, Y. X. Zhao, T. Bian, Y. F. Zhao, C. Zhou, G. I. N. Waterhouse, L. Z. Wu, C. H. Tung and T. R. Zhang, *Adv. Mater.*, 2017, **29**, 1605148.
- 170 L. Lin, C. Hou, X. Zhang, Y. Wang, Y. Chen and T. He, *Appl. Catal., B*, 2018, **221**, 312–319.
- 171 K. Wada, C. S. K. Ranasinghe, R. Kuriki, A. Yamakata, O. Ishitani and K. Maeda, *ACS Appl. Mater. Interfaces*, 2017, **9**, 23869–23877.
- 172 S. Aoi, K. Mase, K. Ohkubo, T. Suenobu and S. Fukuzumi, *ACS Energy Lett.*, 2017, **2**, 532–536.
- 173 H. Kumagai, G. Sahara, K. Maeda, M. Higashi, R. Abe and O. Ishitani, *Chem. Sci.*, 2017, **8**, 4242–4249.
- 174 K.-L. Bae, J. Kim, C. K. Lim, K. M. Nam and H. Song, *Nat. Commun.*, 2017, **8**, 1156.
- 175 M. Xing, Y. Zhou, C. Dong, L. Cai, L. Zeng, B. Shen, L. Pan, C. Dong, Y. Chai, J. Zhang and Y. Yin, *Nano Lett.*, 2018, **18**, 3384–3390.
- 176 Y. Zhao, Y. Weia, X. Wua, H. Zhenga, Z. Zhao, J. Liu and J. Li, *Appl. Catal., B*, 2018, **226**, 360–372.
- 177 S. Wanga, Y. Guan, L. Lu, Z. Shi, S. Yan and Z. Zou, *Appl. Catal., B*, 2018, **224**, 10–16.
- 178 R. Long, Y. Li, Y. Liu, S. Chen, X. Zheng, C. Gao, C. He, N. Chen, Z. Qi, L. Song, J. Jiang, J. Zhu and Y. Xiong, *J. Am. Chem. Soc.*, 2017, **139**, 4486–4492.
- 179 J. K. Stolarczyk, S. Bhattacharyya, L. Polavarapu and J. Feldmann, *ACS Catal.*, 2018, **8**, 3602–3635.
- 180 S. Neațu, J. A. Maciá-Agulló, P. Concepción and H. Garcia, *J. Am. Chem. Soc.*, 2014, **136**, 15969–15976.
- 181 J.-C. Wang, L. Zhang, W.-X. Fang, J. Ren, Y.-Y. Li, H.-C. Yao, J.-S. Wang and Z.-J. Li, *ACS Appl. Mater. Interfaces*, 2015, **7**, 8631–8639.
- 182 S. Das, S. Kumar, S. Garai, R. Pochamoni, S. Paul and S. Roy, *ACS Appl. Mater. Interfaces*, 2017, **9**, 35086–35094.
- 183 T. Arai, S. Sato and T. Morikawa, *Energy Environ. Sci.*, 2015, **8**, 1998–2002.
- 184 A. Iwase, S. Yoshino, T. Takayama, Y. H. Ng, R. Amal and A. Kudo, *J. Am. Chem. Soc.*, 2016, **138**, 10260–10264.

